

## Experimental Detection of Quantum Channel Capacities

Álvaro Cuevas,<sup>1</sup> Massimiliano Proietti,<sup>2,1</sup> Mario Arnolfo Ciampini,<sup>1</sup> Stefano Duranti,<sup>1,3</sup>

Paolo Mataloni,<sup>1</sup> Massimiliano F. Sacchi,<sup>4</sup> and Chiara Macchiavello<sup>5</sup>

<sup>1</sup>Quantum Optics Group, Dipartimento di Fisica, Università di Roma La Sapienza, Piazzale Aldo Moro 5, I-00185 Roma, Italy

<sup>2</sup>Edinburgh Mostly Quantum Lab, School of Engineering and Physical Sciences,

Heriot-Watt University, David Brewster Building, EH14 4AS Edinburgh, United Kingdom

<sup>3</sup>Dipartimento di Fisica e Geologia, Università degli Studi di Perugia, Via Pascoli snc, I-06123 Perugia, Italy

<sup>4</sup>Istituto di Fotonica e Nanotecnologie—Consiglio Nazionale delle Ricerche,

Piazza Leonardo da Vinci 32, I-20133 Milano, Italy

<sup>5</sup>Dipartimento di Fisica, Università di Pavia, and INFN—Sezione di Pavia Via A. Bassi 6, I-27100 Pavia, Italy

(Received 22 December 2016; published 8 September 2017)

We present an efficient experimental procedure that certifies nonvanishing quantum capacities for qubit noisy channels. Our method is based on the use of a fixed bipartite entangled state, where the system qubit is sent to the channel input. A particular set of local measurements is performed at the channel output and the ancilla qubit mode, obtaining lower bounds to the quantum capacities for any unknown channel with no need of quantum process tomography. The entangled qubits have a Bell state configuration and are encoded in photon polarization. The lower bounds are found by estimating the Shannon and von Neumann entropies at the output using an optimized basis, whose statistics is obtained by measuring only the three observables  $\sigma_x \otimes \sigma_x$ ,  $\sigma_y \otimes \sigma_y$ , and  $\sigma_z \otimes \sigma_z$ .

DOI: 10.1103/PhysRevLett.119.100502

*Introduction.*—Any communication channel is unavoidably affected by noise that limits its ability to transmit information, quantified in terms of channel capacity. When the use of the channel aims to convey quantum information, its efficiency is evaluated in terms of the quantum capacity, which is the maximum number of qubits that can be reliably transmitted per channel use [1–4] and represents a central quantitative notion in quantum communications. In general, the computation of the quantum capacity is a hard task, since it requires a regularization procedure over an infinite number of channel uses, and it is therefore by itself not directly accessible experimentally. Its analytical value is known mainly for some channels that have the property of degradability [5–7], since regularization is not needed in this case.

In this Letter, we address the issue of experimental detection of quantum channel capacities. For a generic unknown channel, the quantum capacity can be, in principle, estimated via quantum process tomography [8–18], which provides a complete reconstruction of the channel and therefore leads to an evaluation of all its communication properties. This, however, is a demanding procedure in terms of the number of required different measurement settings, since it scales as  $d^4$  for a finite  $d$ -dimensional quantum system. Moreover, being an indirect method, it also has the drawback of involving larger errors due to error propagation.

Here, we are not interested in reconstructing the complete form of the noise affecting the channel but only in detecting its quantum capacity, which is a very specific

feature for which we developed a novel and less demanding procedure in terms of resources (measurements) involved. This is pursued in the same spirit as it is done, for example, in entanglement detection for composite systems [19], in parameter estimation procedures [20], and in the detection of specific properties of quantum channels, such as being entanglement breaking [21] or non-Markovian [22].

In this Letter, we report the first experiment where a lower bound to the quantum channel capacity is directly accessed by means of a number of local measurements that scales as  $d^2$ , hence more favorably with respect to process tomography that scales as  $d^4$ . The experiment is based on a recently proposed theoretical method [23] that can be applied to generally unknown noisy channels in an arbitrary finite dimension and has been proved to be very efficient for many examples of qubit channels [24].

The method is suited for any kind of physical system available for quantum communication, and the experiment we present here is based on a quantum optical implementation for various forms of noisy single-qubit channels.

*Lower bound on quantum channel capacity.*—The quantum capacity  $Q$  of a noisy channel  $\mathcal{E}$ , measured in qubits per channel use, is defined as [1–4]

$$Q = \lim_{N \rightarrow \infty} \frac{Q_N}{N}, \quad (1)$$

where  $N$  is the number of channel uses,  $Q_N = \max_{\rho} I_c(\rho, \mathcal{E}_N)$ , with  $\mathcal{E}_N = \mathcal{E}^{\otimes N}$ , and  $I_c(\rho, \mathcal{E}_N)$  denotes the coherent information [25]

$$I_c(\rho, \mathcal{E}_N) = S[\mathcal{E}_N(\rho)] - S_e(\rho, \mathcal{E}_N). \quad (2)$$

In the above equation,  $S(\rho) = -\text{Tr}[\rho \log_2 \rho]$  is the von Neumann entropy and  $S_e(\rho, \mathcal{E})$  represents the entropy exchange [26], i.e.,  $S_e(\rho, \mathcal{E}) = S[(\mathcal{I}_R \otimes \mathcal{E})(|\Psi_\rho\rangle\langle\Psi_\rho|)]$ , where  $|\Psi_\rho\rangle$  denotes any purification of  $\rho$  by means of an ancilla reference quantum system  $A$ , namely,  $\rho = \text{Tr}_A[|\Psi_\rho\rangle\langle\Psi_\rho|]$ .

The following chain of bounds holds:

$$Q \geq Q_1 \geq I_c(\rho, \mathcal{E}_1) \geq Q_{\text{DET}}, \quad (3)$$

where the first two inequalities come directly from the above definitions, while the last one was proved in Ref. [23], with

$$Q_{\text{DET}} = S[\mathcal{E}(\rho)] - H(\vec{p}). \quad (4)$$

Here  $\mathcal{E}(\rho)$  is the output state for a single use of the channel, and  $H(\vec{p})$  denotes the Shannon entropy for the vector of the probabilities  $\{p_i\}$  corresponding to a measurement on orthogonal projectors  $\{|\Phi_i\rangle\}$  in the tensor product of the ancilla and the system Hilbert spaces:

$$p_i = \text{Tr}[(\mathcal{I}_A \otimes \mathcal{E})(|\Psi_\rho\rangle\langle\Psi_\rho|)|\Phi_i\rangle\langle\Phi_i|]. \quad (5)$$

The procedure to detect the lower bound  $Q_{\text{DET}}$  is the following: (i) Prepare a bipartite pure state  $|\Psi_\rho\rangle$ ; (ii) send it through the channel  $\mathcal{I}_A \otimes \mathcal{E}$ , where the unknown channel  $\mathcal{E}$  acts on one of the two subsystems; (iii) measure suitable local observables on the joint output state in order to estimate  $S[\mathcal{E}(\rho)]$  and  $\vec{p}$  and to compute  $Q_{\text{DET}}$ . After the measurements have been performed, the detected bound  $Q_{\text{DET}}$  can then be optimized over all probability distributions that can be obtained from the used measurement settings. This last step is achieved by performing an ordinary classical processing of the measurement outcomes. We now specify our scenario to qubit channels ( $d=2$ ), where the protocol requires only  $d^2 - 1 = 3$  observables, in our case  $\sigma_x \otimes \sigma_x$ ,  $\sigma_y \otimes \sigma_y$ , and  $\sigma_z \otimes \sigma_z$  on both the ancilla and system qubit. We also consider a maximally entangled input state  $|\Phi^+\rangle = 1/\sqrt{2}(|00\rangle + |11\rangle)$ . The schematic representation of the procedure is shown in Fig. 1. The above observables allow one to measure  $\{\sigma_i\}$  on the system alone by ignoring the statistics of the measurement results on the ancilla. Since this set is tomographically complete, the system output state  $\mathcal{E}(\rho)$  can be reconstructed, and therefore the term  $S[\mathcal{E}(\rho)]$  in Eq. (4) can be exactly estimated. Moreover, the measurement settings  $\{\sigma_x \otimes \sigma_x, \sigma_y \otimes \sigma_y, \sigma_z \otimes \sigma_z\}$  allow us to estimate the vector  $\vec{p}$  pertaining to the projectors onto the following inequivalent bases [23]:

$$\begin{aligned} B_1 &= \{|B_{1,1}\rangle, |B_{1,2}\rangle, |B_{1,3}\rangle, |B_{1,4}\rangle\} \\ &= \{a|\Phi^+\rangle + b|\Phi^-\rangle, -b|\Phi^+\rangle + a|\Phi^-\rangle, \\ &\quad c|\Psi^+\rangle + d|\Psi^-\rangle, -d|\Psi^+\rangle + c|\Psi^-\rangle\}; \end{aligned} \quad (6)$$

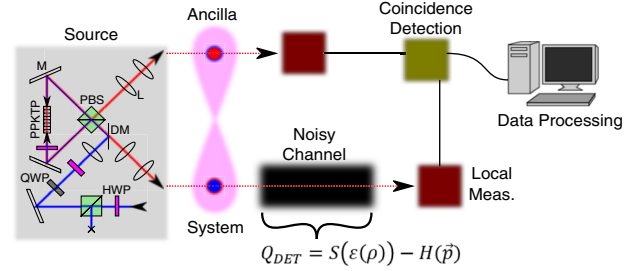


FIG. 1. Experimental setup. A Sagnac interferometric source of polarization-entangled photons sends the  $S$  qubit through the noisy channel, while the  $A$  qubit remains untouched. Both qubits are measured in a joint photon counter system. Here PPKTP is a periodically poled potassium titanyl phosphate nonlinear crystal, PBS a polarizing beam splitter,  $M$  a mirror,  $L$  a converging lens, HWP a half-wave plate, QWP a quarter-wave plate, and DM a dichroic mirror.

$$\begin{aligned} B_2 &= \{|B_{2,1}\rangle, |B_{2,2}\rangle, |B_{2,3}\rangle, |B_{2,4}\rangle\} \\ &= \{a|\Phi^+\rangle + b|\Psi^+\rangle, -b|\Phi^+\rangle + a|\Psi^+\rangle, \\ &\quad c|\Phi^-\rangle + d|\Psi^-\rangle, -d|\Phi^-\rangle + c|\Psi^-\rangle\}; \end{aligned} \quad (7)$$

$$\begin{aligned} B_3 &= \{|B_{3,1}\rangle, |B_{3,2}\rangle, |B_{3,3}\rangle, |B_{3,4}\rangle\} \\ &= \{a|\Phi^+\rangle + ib|\Psi^-\rangle, ib|\Phi^+\rangle + a|\Psi^-\rangle, \\ &\quad c|\Phi^-\rangle + id|\Psi^+\rangle, id|\Phi^-\rangle + c|\Psi^+\rangle\}; \end{aligned} \quad (8)$$

where  $|\Phi^\pm\rangle = 1/\sqrt{2}(|00\rangle \pm |11\rangle)$  and  $|\Psi^\pm\rangle = 1/\sqrt{2}(|01\rangle \pm |10\rangle)$  denote the Bell states and  $a, b, c$ , and  $d$  are real numbers, such that  $a^2 + b^2 = c^2 + d^2 = 1$ .

The evaluation of the Shannon entropy  $H(\vec{p})$  in the  $B_i$  basis is obtained from its definition

$$H(\vec{p}_i) = -\sum_j p_{i,j} \log_2 p_{i,j}, \quad (9)$$

where  $\vec{p}_i = \{p_{i,j}\}$  is the probability vector associated to  $(\mathcal{I}_A \otimes \mathcal{E})(|\Phi^+\rangle\langle\Phi^+|)$ , described in Eq. (5).

The probability vectors can be obtained by measuring the expression  $p_{i,j} = \langle \Pi_{i,j} \rangle$  as described in Supplemental Material [27], with  $\Pi_{i,j} = |B_{i,j}\rangle\langle B_{i,j}|$  the projector on the specific basis element  $|B_{i,j}\rangle$ . All expectation values  $\langle \rangle$  are evaluated for the joint output state  $(\mathcal{I}_A \otimes \mathcal{E})(|\Phi^+\rangle\langle\Phi^+|)$ , and, using the normalization constraints among  $a, b, c$ , and  $d$ , it can be demonstrated that all probabilities  $p_{i,j}$  depend only on two real parameters,  $b$  and  $d$ . After collecting the measurement outcomes, the bound on  $Q$  is then maximized over the three bases  $B_1, B_2$ , and  $B_3$  and by varying  $b$  and  $d$ :

$$\begin{aligned} Q_{\text{DET}} &= \max_{i=1,2,3} \max_{b,d} Q_{\text{DET}}(B_i, b, d) \\ &= S[\mathcal{E}(\rho)] - \min_{i=1,2,3} \min_{b,d} H[\vec{p}(B_i, b, d)]. \end{aligned} \quad (10)$$

This last step is performed by classical processing of the measurement outcomes, from which the set of expectation

values  $\{\langle \mathbb{1} \otimes \sigma_\alpha \rangle, \langle \sigma_\alpha \otimes \mathbb{1} \rangle, \langle \sigma_\alpha \otimes \sigma_\alpha \rangle, \alpha = x, y, z\}$  is obtained. Differently from complete process tomography, we remark that we do not need to measure the six observables of the kind  $\sigma_\alpha \otimes \sigma_\beta$  with  $\alpha \neq \beta$  and, moreover, the bound is directly obtained from the measured expectations, without the need of a linear inversion and/or maximum likelihood technique. Let us also notice that the use of an entangled input state in our procedure is not mandatory. In fact, the ancilla is locally measured, and this is equivalent to heralding a single-photon state at the channel [29].

*Experimental procedure.*—We implemented the method using a spontaneous parametric down conversion (SPDC) source of high-purity polarization-entangled photons [30] schematically represented in Fig. 1, where the qubits were encoded as  $\{|0\rangle \equiv |H\rangle, |1\rangle \equiv |V\rangle\}$ , with  $|H\rangle$  ( $|V\rangle$ ) the horizontal (vertical) polarization.

From a continuous wave laser pumping at 405 nm and bandwidth  $<0.01$  pm, we generate down-converted pairs of single photons at 810 nm and bandwidth  $\approx 0.42$  nm, hence entangled in Bell states with a measured fidelity of  $F_{\text{exp}} = 0.979 \pm 0.011$ , calculated as reported in Ref. [27] and using standard tomography analysis [28]. The entanglement degree of the generated photons corresponds to an average concurrence value of  $C_{\text{exp}} = 0.973 \pm 0.004$  [31].

The input state is ideally the maximally entangled state  $|\Phi^+\rangle$ . Because of experimental imperfections, the resulting state can be described by a Werner state  $\rho_W = (4F - 1/3)|\Phi^+\rangle\langle\Phi^+| + (1 - F/3)I \otimes I$ , where  $F$  is the fidelity with respect to  $|\Phi^+\rangle$ . The derivation of new detectable bounds suited for bipartite input states which are affected by isotropic noise is reported in Ref. [27]. Such bounds will be used to compare our experimental results with the theoretical predictions.

The procedure was tested for the following types of noise: amplitude damping channel (ADC), phase damping channel (PDC), depolarizing channel (DC), and Pauli channel (PC) [32,33]. As remarked above, we employ three versus nine measurements on the output state, as in usual process tomography.

The polarization-based measurement is performed via a QWP, a HWP, and a PBS located in both the reference (ancilla,  $A$ ) and principal system (system,  $S$ ) paths.

The expectation values  $\langle \sigma_\alpha \otimes \sigma_\alpha \rangle$  (with  $\alpha = x, y, z$ ) were obtained by taking every matrix element of  $\sigma_\alpha \otimes \sigma_\alpha$  as a particular projection of the transmitted state [27], which was measured by integrating photon coincidences during a time interval of 5 sec. Since only a set of 12 measurements of the state are needed (four by each of the three observables), the  $Q_{\text{DET}}$  can be obtained in only 60 s. See [27] for information about actual photon count rates and detection efficiencies.

An ADC for polarization qubits with probability  $\gamma$  can be written as  $\mathcal{E}(\rho) = K_0 \rho K_0^\dagger + K_1 \rho K_1^\dagger$ , where  $K_0 = |H\rangle\langle H| + \sqrt{1-\gamma}|V\rangle\langle V|$  and  $K_1 = \sqrt{\gamma}|H\rangle\langle V|$ . The experimental setup [34] consists in a Sagnac interferometer (SI) followed by a

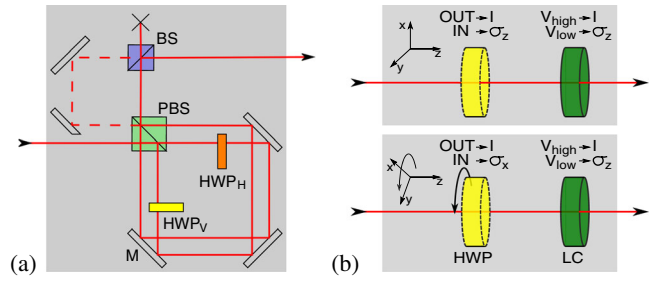


FIG. 2. Noisy channels. (a) Experimental scheme for a polarization ADC. Given a single input qubit  $|\psi\rangle = \alpha|H\rangle + \beta|V\rangle$ , it uses two HWPs inside a SI to apply a rotation on  $|V\rangle$ , while  $|H\rangle$  remains unrotated, achieving  $K_0$  and  $K_1$ . The dashed line inside the MZI represents the rotated  $\sqrt{\gamma}$  portion of  $|V\rangle$ . (b) Top: Experimental scheme for a PDC. It applies  $\mathbb{1}$  and  $\sigma_z$  over  $|\psi\rangle$  by using an unrotated HWP and a variable voltage LC. Bottom: Experimental scheme for the PC and DC. They apply  $\mathbb{1}$ ,  $\sigma_x$ ,  $\sigma_y$ , and  $\sigma_z$  over  $|\psi\rangle$  by using a 45°-rotated HWP and the same LC.

Mach-Zehnder interferometer (MZI), as shown in Fig. 2(a), that allows us to perform the required noise operation. In the Sagnac loop, composed by a PBS and three mirrors, a HWP at  $0^\circ$  is put on the path of polarization  $|H\rangle$ , whereas a HWP at  $\theta$  is put on the path of polarization  $|V\rangle$ . The MZI recombines the two outputs of the SI in a noncoherent superposition within a beam splitter (BS), thus effectively performing the damping operation, whose amount  $\gamma$  depends on the angle  $\theta$  [35].

A PDC for qubits with probability  $p$  can be written as  $\mathcal{E}(\rho) = [1 - (p/2)]\rho + (p/2)\sigma_z\rho\sigma_z$ . This map is achieved by using a sequence of two wave retarders: a HWP at  $0^\circ$ , which acts as  $\sigma_z$ , and an unrotated liquid crystal (LC), which acts as  $\mathbb{1}$  or  $\sigma_z$  depending on the applied voltage on the material [31]. The system qubit is sent through the combination of these two optical elements, suffering a  $\sigma_z\sigma_z = \mathbb{1}$  or  $\mathbb{1}\sigma_z = \sigma_z$  operation, while the ancilla qubit remains untouched. In Fig. 2(b), top, we show the schematic representation of the channel. The probabilities  $P_z = (p/2)$  and  $P_{\mathbb{1}} = 1 - P_z = 1 - (p/2)$  are applied in postprocessing, by evaluating the ratios of photon coincidences from two separated experiments,  $\sigma_z$  and  $\mathbb{1}$ , respectively. Therefore, the total channel corresponds to a mixture of two operations constrained by  $P_z + P_{\mathbb{1}} = 1$ .

A DC for qubits with probability  $p$  can be written as  $\mathcal{E}(\rho) = (1 - p)\rho + (p/3)(\sigma_x\rho\sigma_x + \sigma_y\rho\sigma_y + \sigma_z\rho\sigma_z)$ . The operations are achieved by the presence (absence) of a rotated HWP acting as  $\sigma_x$  when it is on the optical path or acting as  $\mathbb{1}$  if taken off from the path, and by an unrotated LC acting as  $\mathbb{1}$  or  $\sigma_z$ , depending on the applied voltage. From the simultaneous actions of the HWP and the LC over  $\rho$ , the operations can be  $\mathbb{1} = \mathbb{1}$ ,  $\sigma_z\mathbb{1} = \sigma_z$ ,  $\sigma_z\sigma_x = i\sigma_y$ , and  $\mathbb{1}\sigma_x = \sigma_x$ . In Fig. 2(b), bottom, we show the schematic representation of the channel. Analogously to the procedure followed for the PDC, the effective  $\sigma_z$ ,  $\sigma_y$ ,  $\sigma_x$ , and  $\mathbb{1}$  operations were applied in four separate experiments,

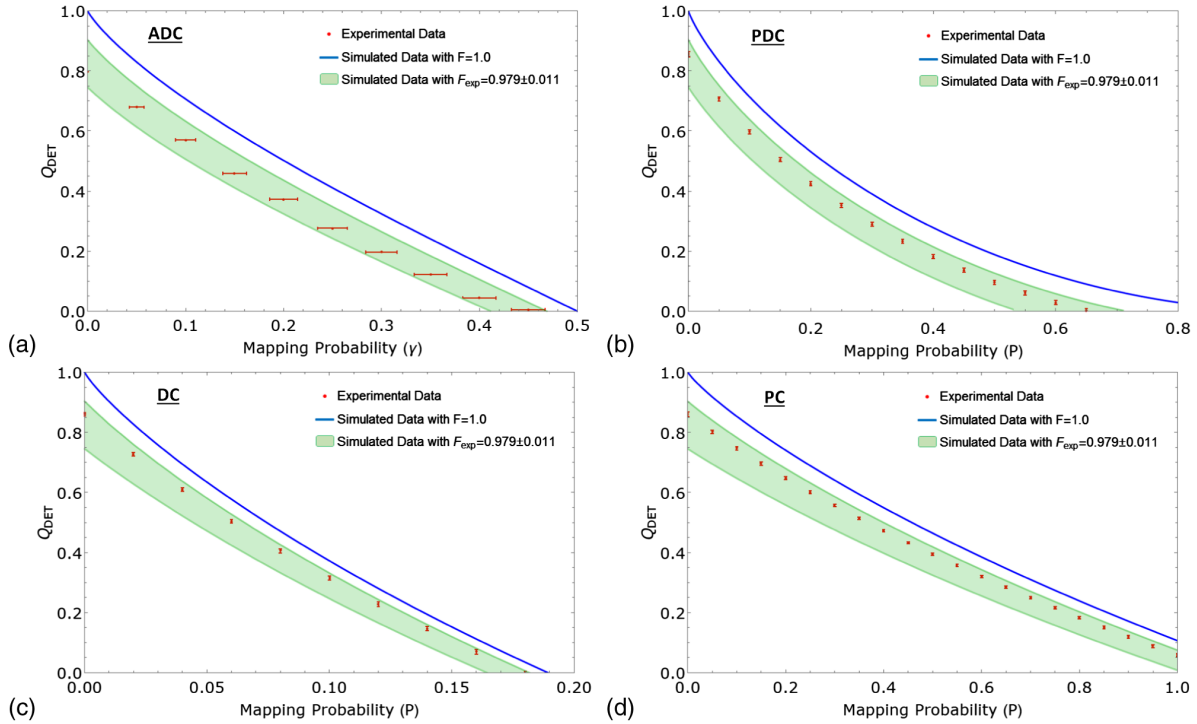


FIG. 3. Minimal bounds  $Q_{\text{DET}}$  to the quantum channel capacity. For the entire set of data, the red points represent the experimental values, and the continuous blue line corresponds to the ideal simulation of a pure input state  $|\Phi^+\rangle$  with fidelity  $F = 1$ . Green shaded areas correspond to a region of  $Q_{\text{DET}}$  for an input Werner state  $\rho_W$  within one standard deviation of fidelity  $F_{\text{exp}} = 0.979 \pm 0.011$ . (a) ADC:  $Q_{\text{DET}}$  versus the damping parameter  $\gamma$ . (b) PDC:  $Q_{\text{DET}}$  versus  $p$  for the statistical mixture of  $\mathbb{I}$  and  $\sigma_z$ , with probability vector  $\vec{p} = \{P_{\mathbb{I}}, P_x, P_y, P_z\} = [1 - (p/2), 0, 0, (p/2)]$ . (c) DC:  $Q_{\text{DET}}$  versus  $p$  for the balanced mixture of  $\mathbb{I}$ ,  $\sigma_x$ ,  $\sigma_y$ , and  $\sigma_z$ , with  $\vec{p} = [1 - p, (p/3), (p/3), (p/3)]$ . (d) PC:  $Q_{\text{DET}}$  versus  $p$  for the mixture of  $\mathbb{I}$ ,  $\sigma_x$ ,  $\sigma_y$ , and  $\sigma_z$ , with  $\vec{p} = [1 - (p/6), (p/12), (p/18), (p/36)]$ . The error bars on the mapping probability are significant only in case (a), where an uncertainty of  $0.5^\circ$  in the rotation angle of  $\text{HWP}_V(\gamma)$  was propagated, while this error was negligible in cases (b)–(d). In case (a), the error bars on  $Q_{\text{DET}}$  were calculated from Poissonian statistics on one set of points, obtaining negligible values. In cases of (b)–(d), error bars were obtained from an average of at least eight sets of points. (See [27] for more details.)

where  $P_z = P_y = P_x = (p/3)$  and  $P_{\mathbb{I}} = 1 - p$  were added in postprocessing of the experimental outcomes.

The PC for qubits with probability  $p$  can be written as  $\mathcal{E}(\rho) = P_{\mathbb{I}}\rho + P_x\sigma_x\rho\sigma_x + P_y\sigma_y\rho\sigma_y + P_z\sigma_z\rho\sigma_z$  and has been implemented by the same procedure used for the DC. However, in this case there is no restriction on the choice of  $P_i$  except for the condition  $P_{\mathbb{I}} + P_z + P_y + P_x = 1$ , also valid for DC.

**Results.**—In Fig. 3, we show the experimental measurements of  $Q_{\text{DET}}$  for a prepared ADC, PDC, DC, and PC. The experimental values are in very good agreement with the theoretical predictions.

These results prove the effectiveness of the method, which assesses efficiently the lower bound of  $Q_{\text{DET}}$  to the quantum capacity of noisy channels with the most common kinds of noise.

Moreover, the well-known expressions for the ADC and PDC quantum capacities [5,36] coincide with our detectable bound. The expected nonzero capacity for the ADC occurs when  $\gamma < 1/2$ , while the certified experimental value was  $\gamma < 0.45$  [see Fig. 3(a)]. For the PDC, we obtained a nonvanishing value of the  $Q_{\text{DET}}$  for values of

$p$  up to 0.65, whereas the ideal analytical expression is positive for any value of  $p$  [see Fig. 3(b)].

In the case of DC, the procedure certifies a nonzero channel capacity for values of  $p \leq 0.18$ , while the best theoretical lower bound predicts a nonzero channel capacity up to  $p = 0.1892$  [37]. Analogously, the technique certifies a nonzero channel capacity of the chosen PC for any value of  $p$ , similar to the ideal simulated channel.

**Conclusions.**—We have performed an experiment to detect efficient lower bounds to the quantum capacity of qubit communication channels. Our technique does not require any prior knowledge of the quantum channel and can be applied to any kind of unknown noise. The principal feature of the technique resides on the smaller number of measurement settings with respect to full process tomography and is in very good agreement with the theoretical prediction for the source we used. To the best of our knowledge, this is the first experiment where the quantum capacity of a noisy channel is directly accessed. Furthermore, the detectable bounds we have provided give lower bounds to the private information and to the entanglement-assisted classical capacity, as emphasized in Ref. [23].

These results represent an important step toward an efficient experimental characterization of quantum channels such as those used in quantum cryptography, quantum teleportation, and quantum dense coding.

Á.C. thanks the support from the Chilean agency Comisión Nacional de Investigación Científica y Tecnológica and to its Ph.D. scholarship program Becas Chile.

- 
- [1] S. Lloyd, *Phys. Rev. A* **55**, 1613 (1997).  
 [2] H. Barnum, M. A. Nielsen, and B. Schumacher, *Phys. Rev. A* **57**, 4153 (1998).  
 [3] I. Devetak, *IEEE Trans. Inf. Theory* **51**, 44 (2005).  
 [4] P. Hayden, M. Horodecki, A. Winter, and J. Yard, *Open Syst. Inf. Dyn.* **15**, 7 (2008).  
 [5] I. Devetak and P. Shor, *Commun. Math. Phys.* **256**, 287 (2005).  
 [6] J. Yard, I. Devetak, and P. Hayden, *IEEE Trans. Inf. Theory* **54**, 3091 (2008).  
 [7] T. S. Cubitt, M. Ruskai, and G. Smith, *J. Math. Phys. (N.Y.)* **49**, 102104 (2008).  
 [8] I. L. Chuang and M. A. Nielsen, *J. Mod. Opt.* **44**, 2455 (1997).  
 [9] J. F. Poyatos, J. I. Cirac, and P. Zoller, *Phys. Rev. Lett.* **78**, 390 (1997).  
 [10] M. F. Sacchi, *Phys. Rev. A* **63**, 054104 (2001).  
 [11] G. M. D'Ariano and P. Lo Presti, *Phys. Rev. Lett.* **86**, 4195 (2001).  
 [12] J. B. Altepeter, D. Branning, E. Jeffrey, T. C. Wei, P. G. Kwiat, R. T. Thew, J. L. O'Brien, M. A. Nielsen, and A. G. White, *Phys. Rev. Lett.* **90**, 193601 (2003).  
 [13] J. L. O'Brien, G. J. Pryde, A. Gilchrist, D. F. V. James, N. K. Langford, T. C. Ralph, and A. G. White, *Phys. Rev. Lett.* **93**, 080502 (2004).  
 [14] S. H. Myrskog, J. K. Fox, M. W. Mitchell, and A. M. Steinberg, *Phys. Rev. A* **72**, 013615 (2005).  
 [15] M. Riebe, K. Kim, P. Schindler, T. Monz, P. O. Schmidt, T. K. Körber, W. Hänsel, H. Häffner, C. F. Roos, and R. Blatt, *Phys. Rev. Lett.* **97**, 220407 (2006).  
 [16] M. Mohseni, A. T. Rezakhani, and D. A. Lidar, *Phys. Rev. A* **77**, 032322 (2008).  
 [17] I. Bongioanni, L. Sansoni, F. Sciarrino, G. Vallone, and P. Mataloni, *Phys. Rev. A* **82**, 042307 (2010).  
 [18] Y. Sagi, I. Almog, and N. Davidson, *Phys. Rev. Lett.* **105**, 053201 (2010).  
 [19] O. Gühne, P. Hyllus, D. Bruß, A. Ekert, M. Lewenstein, C. Macchiavello, and A. Sanpera, *Phys. Rev. A* **66**, 062305 (2002).  
 [20] G. M. D'Ariano, M. G. A. Paris, and M. F. Sacchi, *Phys. Rev. A* **62**, 023815 (2000).  
 [21] C. Macchiavello and M. Rossi, *Phys. Rev. A* **88**, 042335 (2013); A. Orioux, L. Sansoni, M. Persechino, P. Mataloni, M. Rossi, and C. Macchiavello, *Phys. Rev. Lett.* **111**, 220501 (2013).  
 [22] D. Chruściński, C. Macchiavello, and S. Maniscalco, *Phys. Rev. Lett.* **118**, 080404 (2017).  
 [23] C. Macchiavello and M. F. Sacchi, *Phys. Rev. Lett.* **116**, 140501 (2016).  
 [24] C. Macchiavello and M. F. Sacchi, *Phys. Rev. A* **94**, 052333 (2016).  
 [25] B. W. Schumacher and M. A. Nielsen, *Phys. Rev. A* **54**, 2629 (1996).  
 [26] B. W. Schumacher, *Phys. Rev. A* **54**, 2614 (1996).  
 [27] See Supplemental Material at <http://link.aps.org/supplemental/10.1103/PhysRevLett.119.100502> for a detailed description of theoretical quantum channel capacities, experimental method, photon efficiencies and the error estimation used in the experiment. The file also includes Refs. [23,28].  
 [28] D. F. V. James, P. G. Kwiat, W. J. Munro, and A. G. White, *Phys. Rev. A* **64**, 052312 (2001).  
 [29] This can also be seen by the following identity for the expectations on the bipartite output state  $\langle \sigma_\alpha \otimes \sigma_\beta \rangle = \text{Tr}[(\mathcal{I}_A \otimes \mathcal{E})(|\Phi^+\rangle\langle\Phi^+|)(\sigma_\alpha \otimes \sigma_\beta)] = \frac{1}{2} \text{Tr}[\sigma_\beta \mathcal{E}(\sigma_\alpha^\tau)]$ , where  $\tau$  denotes the transposition. The expectation values  $\langle \sigma_\alpha \otimes \sigma_\alpha \rangle$  and therefore also the probabilities in Eq. (5) can then be obtained by considering only the system qubit, preparing it in the eigenstates of  $\sigma_\alpha^\tau$  with equal probabilities, and measuring  $\sigma_\alpha$  at the output of the channel.  
 [30] A. Fedrizzi, T. Herbst, A. Poppe, T. Jennewein, and A. Zeilinger, *Opt. Express* **15**, 15377 (2007).  
 [31] N. K. Bernardes, Á. Cuevas, A. Orioux, C. H. Monken, P. Mataloni, F. Sciarrino, and M. F. Santos, *Sci. Rep.* **5**, 17520 (2015).  
 [32] M. A. Nielsen and I. L. Chuang, *Quantum Computation and Quantum Information*, 10th anniversary edition (Cambridge University Press, Cambridge, England, 2010).  
 [33] E. Desurvire, *Classical and Quantum Information Theory: An Introduction for the Telecom Scientist* (Cambridge University Press, Cambridge, England, 2009).  
 [34] Á. Cuevas, A. Mari, A. De Pasquale, A. Orioux, M. Massaro, F. Sciarrino, P. Mataloni, and V. Giovannetti, *Phys. Rev. A* **96**, 012314 (2017).  
 [35] M. P. Almeida, F. de Melo, M. Hor-Meyll, A. Salles, S. P. Walborn, P. H. Souto Ribeiro, and L. Davidovich, *Science* **316**, 579 (2007).  
 [36] V. Giovannetti and R. Fazio, *Phys. Rev. A* **71**, 032314 (2005).  
 [37] D. P. Di Vincenzo, P. W. Shor, and J. A. Smolin, *Phys. Rev. A* **57**, 830 (1998).